Raman Scattering from Alkali Graphite Intercalation Compounds

S. A. Solin
Department of Physics, Michigan State University, East Lansing, Michigan, USA

N. Caswell
Department of Physics, The University of California, Berkeley, California, USA

The stage dependences of the Raman spectra of potassium, rubidium and cesium graphite intercalation compounds are reported. The spectra of each set of compounds are found to be qualitatively and quantitatively consistent with the 'nearest layer' model for the carbon intralayer $E_{2g}^{(2)}$ vibrations of intercalation compounds. To within experimental error the charge exchanged from the intercalant layers to the carbon layers is found to be stage independent and partially localized in type *B* carbon layers which are contiguous to intercalant layers. The relative Raman cross-section for scattering from type *B* and type *C* (noncontiguous) carbon layers is found to be species independent and is $\sigma_C/\sigma_B = 0.25 \pm 0.05$.

INTRODUCTION

Graphite, the prototypical lamellar compound can ingest whole layers of atomic or molecular species into the interlayer spaces separating the carbon layer planes.[1] Moreover, the carbon planes retain their basic layer confirmation after uptake of the guest species. The resultant compounds are called graphite intercalation compounds (GICs) and can be characterized by their electronic, chemical or stoichiometric, and structural properties.

The intercalation process generally involves charge transfer between the graphite layers and the intercalant.[2] When electronic charge is transferred from the intercalant to the carbon layers as it is for the alkali metal intercalants K, Rb or Cs the resultant compounds are labeled donor compounds. Similarly, when electronic charge is transferred to the intercalant layers from the host layers as in the case of molecular intercalants such as SbF_5, HNO_3 etc. the resultant compounds are classified as acceptor compounds.

As with other guest–host solid systems, the stoichiometry of graphite intercalation compounds is an important parameter. In fact, two stoichiometries are often specified for GICs, the bulk stoichiometry specified by the ratio of carbon atoms to guest atoms as, for example, in $C_{24}K$ and the layer stoichiometry which gives the corresponding ratio for the number of carbon atoms in a layer relative to the number of intercalant atoms (or molecules) in an adjacent intercalant layer, e.g. $C_{12}K$. The layer and bulk stoichiometries may or may not be the same and are of course related to the intra- and inter-layer structures of the guest and host species.

It is the structural properties of GICs and, in particular, the property of staging[3] which makes this class of materials unique and which accounts for the recent explosion of interest in them[4,5] (see discussion below). Staging is a phenomena in which, for a given intercalant species, GICs can be prepared with n contiguous carbon layers interspersed between each pair of intercalant layers in a stacking sequence that repeats along the c-axis thus forming a stage n compound where $n = 1, 2, 3, \ldots$. For a few intercalants such as K, Rb, Cs and HNO_3 the above described stacking sequences exhibit long-range order (c-axis correlation lengths in excess of 500 Å) and GICs can be prepared as 'pure' stages.[6] Much more common, however, are impurely staged GICs in which the number of contiguous carbon layers between intercalant layers in an 'impure' stage n compound varies around an average of n.

The spectacular increase in interest in GICs which has developed during the past five years stems not only from their unique staging properties but also from several other novel features. For instance, certain GICs have been shown to exhibit basal plane room temperature conductivities in excess of that of copper.[7] Of more fundamental interest is the possibility of employing GICs to study aspects of two-dimensional physics in a system in which the guest–guest interlayer interaction can be changed stepwise continuously by staging. In this regard recent X-ray diffuse and discreet diffraction studies[8–11] of alkali GICs have revealed a number of interesting intercalant intralayer structures, order–disorder transitions and two-dimensional → three-dimensional crossover phenomena.

While the unusual 'static' or structural properties of GICs are best probed by X-ray diffraction, the dynamic properties are best probed by neutron scattering[12] and or Raman scattering.[13] However, for the study of the vibrational excitations in the optical mode region of GICs Raman scattering is the technique of choice. From the Raman spectra of GICs one can gain significant information on the interlayer and intralayer interactions and, in addition, on the charge exchange and delocalization.

To date, several Raman studies of GICs have been carried out on low-stage $n \leq 3$ donor[13–15] and acceptor[16,17] GICs while only in two cases involving the Rb[18]

CCC-0377-0486/81/0010-0129 $03.50

and $FeCl_3$[19,13,17] intercalants have the full ramifications of staging *vis à vis* light scattering been explored. For the $FeCl_3$ intercalant there is evidence that stages with $n > 1$ are relatively 'impure' in the surface region accessible to the back-scattering Raman technique.[13,20] In contrast, the heavy alkali metals have been known to form pure stages even up to $n = 5$[21] and thus as a class are ideally suited to light-scattering studies. The first detailed study of the stage dependence of the Raman spectra of a GIC was that of stages 1 through 6 Rb–graphite.[18] The purpose of this paper is to report corresponding studies of the K and Cs intercalants and coalesce the information on the heavy alkali intercalates in order that general light-scattering properties of that class of materials might become evident.

EXPERIMENTAL

The samples used in this study were $8 \times 12 \times \approx 0.5$ mm slabs of highly oriented pyrolytic graphite (HOPG).[22] HOPG is a polycrystaline material in which the microcrystal c-axes are essentially parallel while the a-axes are randomly oriented in the basal plane. The mosaic spread of a typical sample was $\approx 0.5°$ before intercalation and 1–2° after.

Graphite samples were cut from large slabs using a wire saw and #600 SiC grit followed by a thorough rinse in acetone and distilled and deionized water. Selected samples were heated to 2100 °C in an induction furnace under a vacuum of 1×10^{-6} torr. This heat treatment had no observable effect on the results of either X-ray or Raman experiments. All graphite pieces were stored in a desiccator. Immediately prior to loading the graphite into a sample preparation tube, an atomicly clean, optical surface was prepared by cleaving off a thin layer from each sample face using Scotch tape.

The alkali metals used were obtained from commercial sources. The potassium was reagent grade packed under mineral oil while the rubidum and cesium were 99.99% pure and were packed under argon.

Since the alkali metals are highly reactive, all manipulations were carried out in a N_2 glove box. To simplify handling and minimize the exposed metallic surface, metals were heated under a vacuum (2×10^{-5} torr) and transferred to 1 mm and i.d. Pyrex tubing. Using this technique a known quantity of metal could be obtained by cutting off a measured length of tubing. Furthermore, only the end surfaces of the metal were exposed to the ambient atomsphere.

Pyrex or fused silica preparation tubes were cleaned according to good high-vacuum practice and loaded with graphite and alkali metal under an N_2 atmosphere. The sample tubes were evacuated, outgassed at 300 °C and sealed at a pressure $\leq 10^{-6}$ torr. After the preparation tube was sealed, the alkali metal was distilled, both to purify the metal and to getter any residual reactive gases in the tube.

Samples were prepared by vapor transport of alkali metal from a reservoir of alkali metal to the graphite sample. The stage of the resulting compound is a function of the vapor pressure of alkali metal over the graphite and the temperature of the graphite. A two-zone furnace was used, in which the metal temperature was controled to give a constant vapor pressure of 10^{-4} torr ($T_{metal} = 250$, 210 and 194 °C for K, Rb and Cs, respectively) and the graphite temperature ($T_{graphite} > T_{metal}$) was independently varied to prepare the desired compound. This standard procedure is referred to as 'the two-bulb method'.[23] The temperatures of the metal and graphite were stable to ±0.25 °C. Separate thermocouples were used for temperature measurement and control.

The sample stage is determined from the c-axis repeat distance measured from the (00l) X-ray reflections. The expected distance is given by the classical model,[3,24]

$$d = N[(n-1)3.35 + d_M] \text{ Å} \quad (1)$$

where d_M is a characteristic constant of each intercalant, 3.35 Å is the separation of carbon layers in pristine graphite[25], n is the stage, N is an integer depending on the c-axis stacking sequence and d is the c-axis repeat distance. Recently, the assumption that d_M is independent of stage has been shown to be incorrect.[26] However the variations in d_M are small, and for the purpose of stage characterization Eqn (1) is adequate. Values of d_M for $M = K$, Rb and Cs are 5.35, 5.65 and 5.94 Å, respectively.[27] Diffraction patterns for the (00l) reciprocal lattice lines of the potassium GICs are shown in Fig. 1. Similar patterns have been obtained for the Rb and Cs intercalants. Notice from Fig. 1 that the (00l) reflections of the higher stage compounds have widths comparable to the reflections from the stage one compound C_8K. This fact and a careful consideration of the spectral profiles of the (00l) reflections shown in Fig. 1 indicate that the alkali GICs do indeed form 'pure' stages. The diffraction patterns of Fig. 1 were obtained

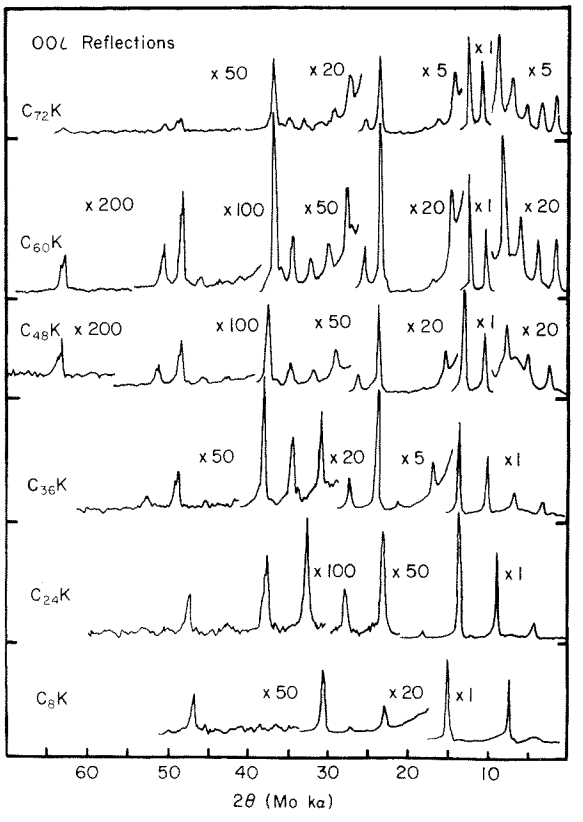

Figure 1. Typical (00l) diffraction patterns from K-GICs used to characterize the sample stage. Stoichiometries listed obey the formula $C_{12n}K$, where n is the stage, with the exception of stage 1 which has the chemical formula C_8K.

using a powder diffractometer and filtered MoKα radiation. A sample was accepted as a stage n when every stage n reflection at $2\theta > 25°$ was observable and no reflection from stage $n \pm 1$ could be detected.

Raman spectra were obtained at room temperature in the back scattering configuration[28] using 5145 Å argon ion laser radiation. A line image was used to minimize the power density at the sample surface. With a laser image size of 0.01×5 mm on the sample, deterioration of stage 1 samples was observed when the laser power exceeded 50, 100 and 300 mW for stage 1 K–, Rb– and Cs–graphite, respectively. The deterioration manifested itself in the appearance of stage 2 spectral features in a stage 1 spectrum. In K– and Rb–graphite the damage was irreversible, with a blue stage 2 region remaining after the laser power was removed. In Cs–graphite the damage anealed at room temperature within minutes. Although the damage threshold for higher stage compounds is higher, all spectra reported here were obtained with power densities lower than that observed to damage a stage 1 compound.

RESULTS AND DISCUSSION

Pristine graphite

In order to discuss fully the Raman spectra of intercalated graphite it is of course necessary to understand the parent spectra of pristine graphite. The hexagonal form of pristine graphite crystallizes in the space group D^4_{6h} with four atoms and two layers per primitive cell.[25] Group theoretical calculations indicate that the zone-center optic modes can be decomposed into the following irreducible representations:[29]

$$\Gamma_{opt} = 2E_{2g} + E_{1u} + A_{2u} + 2B_{2g} \qquad (2)$$

Of these, the E_{2g} modes are Raman-active, the E_{1u} and A_{2u} modes are IR-active and the B_{2g} modes are silent. The Raman-active modes can be further designated as $E^{(1)}_{2g}$, a rigid layer shear mode, and $E^{(2)}_{2g}$ the intralayer mode. The former has until very recently[30] escaped detection. Both Raman-active modes and their corresponding eigenvectors[31] are shown in Fig. 2. With the recent observation and identification of the A_{2u} mode[32] the symmetries and numbers of all four optically active modes have now been confirmed and conform perfectly to the group theoretical predictions given in Eqn (2).

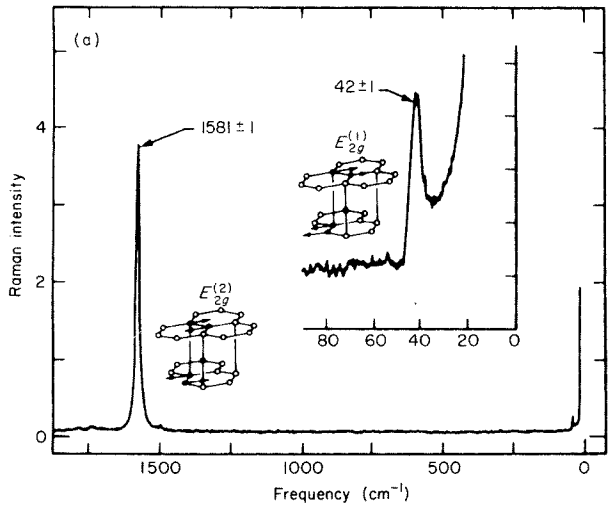

Figure 2. Raman-active modes and atomic displacements of pristine hexagonal graphite from Ref. 30.

Intercalated graphite

The spectral region below 100 cm^{-1} for alkali GICs exhibits intense continuum scattering which is derived both from parasitic radiation and a real background that has been identified as a disorder-induced single-phonon continuum.[33] Thus no evidence has yet been found for a low-frequency '$E^{(1)}_{2g}$-like' mode from GICs. For this reason and also because the $E^{(2)}_{2g}$ graphitic mode is very sensitive to the presence of intercalant species we will focus on the $E^{(2)}_{2g}$ mode.

In their original paper on donor compounds of graphite Nemanich *et al.*[34] postulated a 'nearest layer' (NL) model to account for stage-dependent alterations in the $E^{(2)}_{2g}$ mode that result from intercalation of pristine graphite. We briefly summarize the NL model below and we will show that it accounts both qualitatively and quantitatively for the stage dependence of the Raman spectra of heavy alkali GICs.

Consider the possible nearest layer environments of the carbon layers in a pure stage n intercalation compound as depicted in Fig. 3. In a stage 1 compound each carbon layer is bounded by a pair of intercalate layers (Fig. 3(a)); there is only one nearest layer environment which we label type A. Similarly, in a stage 2 compound, each carbon layer is bounded by another carbon layer and an intercalate layer (Fig. 3(b)), again there is only one nearest layer environment but it differs from that in a stage 1 compound and is labeled type B. In a stage n compound, $n \geq 3$, there are just two types of nearest layer environments, one of type B which is identical to the environment in a stage 2 compound and one labeled type C in which a carbon layer is bounded by other carbon layers as in the case of pristine graphite (see Fig. 3(c)).

Suppose now that the intralayer $E^{(2)}_{2g}$ mode of pristine graphite is sensitive to the nearest layer environment. Since the carbon hexagon layer structure is, to first order, undistorted in an intercalation compound,[1] the atomic displacements corresponding to the $E^{(2)}_{2g}$ mode will also occur in an intercalated sample but the force constants which determine the mode frequency will

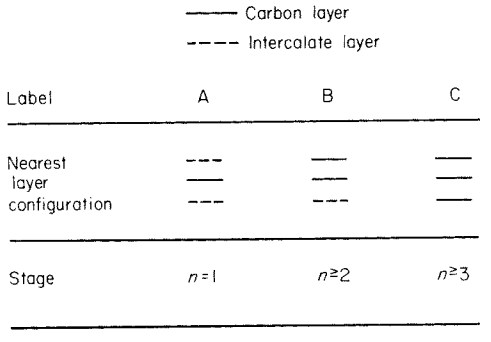

Figure 3. Nearest layer environments of graphite layers in graphite intercalation compounds showing: (a) A-type layers in stage 1 compounds; (b) B-type layers in stage 2 compounds; (c) C-type layers (along with B-type layers) in stage $n (n \geq 3)$ compounds.

depend on the nearest layer environment. Therefore the nearest layer model predicts that a pure stage 1 donor or acceptor compound should exhibit a single Raman band in the vicinity of, but displaced in frequency from, the $E_{2g}^{(2)}$ mode of pristine graphite. The same should be true for a stage 2 compound. However, for stage 3 and higher stage compounds one expects to observe two high-frequency Raman bands, one at the position of the $E_{2g}^{(2)}$ pristine graphite mode and one displaced in frequency. Furthermore, the two bands which result respectively from type B and type C environments in stage n, $n \geq 3$ compounds should exchange intensity, the type C band at the position of the $E_{2g}^{(2)}$ pristine graphite mode becoming more intense with increasing stage number.

This latter point can be simply quantified by 'counting' the number of layers having a particular nearest layer environment in a given stage n compound.[18,35] From such a counting procedure one finds that the relative integrated intensity ratio, R, of type B and type C derived Raman bands for stage $n \geq 2$ donor or acceptor compounds is

$$R \equiv \frac{I_C}{I_B} = \frac{n-2}{2} \times \frac{\sigma_C}{\sigma_B} \tag{3}$$

Here I_B and I_C are, respectively, the intensities of the type B and type C Raman bands and $\sigma_C(\sigma_B)$ is the Raman cross-section for scattering from an $E_{2g}^{(2)}$ type intralayer mode in a type C (type B) layer. Assume that σ_C/σ_B is stage independent which is equivalent to the assumption that the charge transfer to (from) the carbon layer is stage independent in a donor (acceptor) compound. Then R should be a linear function of n that intersects the n axis at $n = 2$ and whose slope yields the Raman cross-section ratio σ_C/σ_B.

The Raman spectra of the stage 1 alkali GICs are shown in Fig. 4. These spectra differ from the Raman spectra of all other GICs measured to date.[34,35,13] The primary source of this distinction is the continuous background extending from $\omega = 0$ to $\omega \geq 3000\ \text{cm}^{-1}$ seen in Fig. 4. The low-frequency region ($\omega \leq 600\ \text{cm}^{-1}$) has been extensively studied for stage 1 C_8Cs[33] and to a lesser extent for C_8K and C_8Rb. Measurement of the temperature dependence of the Stokes–anti-Stokes ratio for the stage 1 Cs compound shows that the continuum in the region below $600\ \text{cm}^{-1}$ is the result of single phonon scattering, possibly activated by stacking disorder.[33] Evidence for the existence of large numbers of stacking faults in stage 1 C_8Cs has been obtained from X-ray diffraction studies.[11]

Superposed on the stage 1 continuum scattering is a triplet of sharp features in the region $550\ \text{cm}^{-1} < \omega < 620\ \text{cm}^{-1}$, one of which interacts with the background to yield a Fano[36] line shape.[33] Another (broad) Fano resonance is observed in the region $1400\ \text{cm}^{-1} < \omega < 1550\ \text{cm}^{-1}$.[34,35] Detailed computer fits to both of the Fano line shapes exhibited by C_8Cs have been carried out[34,37] and the bare frequencies of the discreet states participating in the interaction have been determined. The high-frequency Fano resonances have also been analyzed for C_8K and C_8Rb. The original assumption[34] that the interaction responsible for the resonance at $\approx 1500\ \text{cm}^{-1}$ involves the $1580\ \text{cm}^{-1}$ $E_{2g}^{(2)}$ discreet state has now been verified.[37]

Consider now the low-frequency triplet exhibited in the Raman spectra of stage 1 alkali GICs. As can be seen from Fig. 5(a) the triplet is well resolved for C_8Cs and consists, in order of increasing frequency, of a polarized mode, a depolarized Fano line and a weak depolarized mode. The corresponding features are also evident for RbC_8 (Fig. 5(b)) but the strong polarized mode and Fano line can only be resolved in polarized spectra.[35,33] Note that the weak unpolarized mode, at $\omega \approx 620\ \text{cm}^{-1}$ is not due to spurious effects such as laser florescence or grating ghosts. While not observed in the spectrum of C_8K, this does not preclude its existence. The signal-to-noise ratio of spectra obtained from potassium GICs is low compared to Rb- or Cs-GICs as a direct consequence of the low input power required to avoid sample damage.

The low-frequency triplet of modes observed in stage 1 alkali GICs has been discussed in detail elsewhere.[13,33] Suffice it to say here that it, like the $\omega < 600\ \text{cm}^{-1}$ continuum background, arises from disorder-induced scattering[33] and is quantitatively consistent with recent

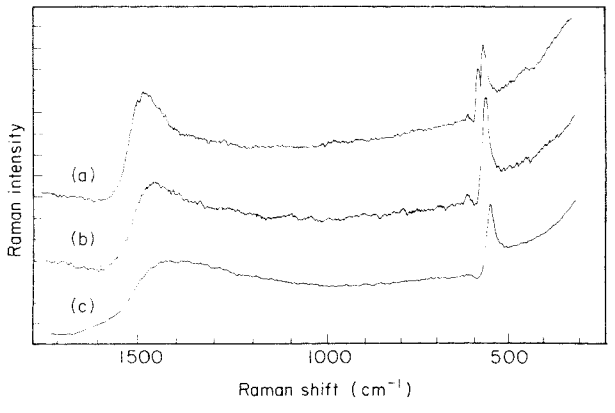

Figure 4. Raman spectra of the stage 1 (a) C_8Cs; (b) C_8Rb; and (c) C_8K with the incident and scattered polarizations parallel to one another and perpendicular to the scattering plane in the ||, || configuration.

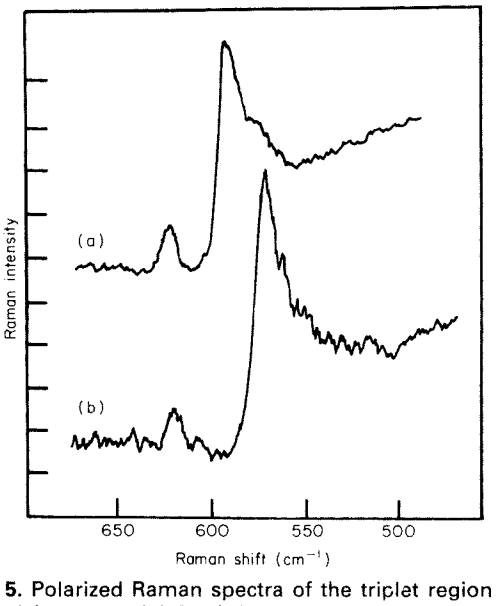

Figure 5. Polarized Raman spectra of the triplet region for the stage 1 (a) Cs; and (b) Rb GICs with the incident polarization perpendicular and the scattered polarization parallel to the scattering plane. Polarized modes (A_g or A_1) are forbidden in this configuration.

Table 1. Frequencies of the stage 1 triplet Raman bands

Sample	Space group of ordered structure	Observed energy[a] (cm^{-1})	Calculated energy[b] (cm^{-1})	Calculated[c] and observed symmetry
C_8K	D_{2h}^{24}	554	582	A_g
		557	583	B_{1g}
		—	592	$A_g + B_{1g}$
C_8Rb	D_{2h}^{24}	566	586	A_g
		573	588	B_{1g}
		617	600	$A_g + B_{1g}$
C_8Cs	D_6^4 or D_6^5	574	—	A_1
		585	—	E_2
		620	—	R_2

[a] These energies are accurate to $\pm 1\ cm^{-1}$.
[b] From Ref. 38.
[c] KC_8 and RbC_8 from Ref. 38, C_sC_8 from Ref. 33.

calculations[38] of the phonon dispersion curves of alkali GICs. These results are summarized in Table 1. Note that the observed energy of the Fano resonance given in Table 1 is the *renormalized* energy. The 'bare' energy of the discreet state which interacts with the continuum to produce the resonance will be higher by ~ 5–$10\ cm^{-1}$. For stage 1 C_8Cs for example the bare energy is upshifted by $9\ cm^{-1}$ to $594\ cm^{-1}$.

The Raman spectra for stage n, $n \geq 2$ alkali GICs are exemplified by the spectra for K-GICs shown in Figs 6 and 7 and are in accordance with the predictions of the NL model. These spectra are in fact typical of all GICs with the exception of stage 1 alkali GICs. In Fig. 6 the only structure above counter noise is a single feature at $1610\ cm^{-1}$ in stage 2 $C_{24}K$ that evidences a weak Fano interaction, and a doublet in the same region for stage n, $n \geq 3$. The singlet in stage 2 and the higher-frequency component of the doublet arise from the graphite $E_{2g}^{(2)}$-like mode from B-type carbon layers while the lower-frequency member of the doublet arises from the $E_{2g}^{(2)}$ mode of unperturbed, C-type layers.

A two-Lorentzian least squares fit has been performed on the Raman spectra of stages 2–6 K-, Rb- and Cs-GICs. Typical fits are shown for K-GICs in Fig. 7, and the best fit parameters for all of the heavy alkali GICs have been listed in Table 2.

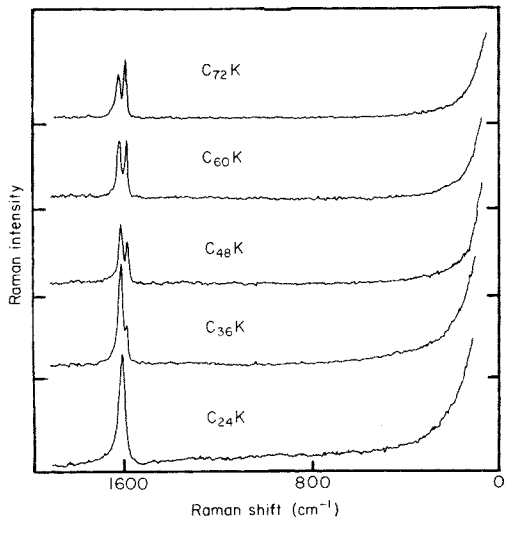

Figure 6. Raman spectra of stage n, $n \geq 2$ K-GICs with compositions $C_{12n}K$.

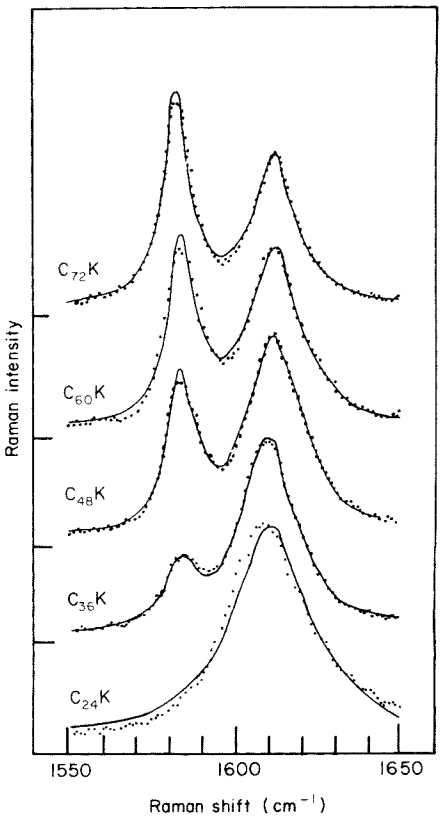

Figure 7. Raman spectra of the doublet region of stage n, $n \geq 2$ K-GICs showing the experimental data (●) and the two Lorentzian least squares fit (——). The parameters of this fit for K-, Rb- and Cs-GICs are tabulated in Table 2.

Table 2. Parameters of the Lorentzian fits to the Raman spectra of stage n, $n \geq 2$ alkali GICs[a]

Sample	ω_C	Y_C	Γ_C	ω_B	Y_B	Γ_B	R
$C_{24}K$	—	—	—	1610	22.3	26.0	0
$C_{36}K$	1584	5.7	6.9	1610	20.4	18.6	0.10
$C_{48}K$	1584	4.5	7.0	1612	12.6	18.7	0.28
$C_{60}K$	1584	11.6	7.4	1612	11.3	17.8	0.43
$C_{72}K$	1583	22.6	6.7	1613	16.2	13.8	0.68
$C_{24}Rb$	—	—	—	1603	17.2	22.0	0
$C_{36}Rb$	1582	3.8	8.3	1606	13.7	14.9	0.15
$C_{48}Rb$	1582	6.0	8.3	1609	13.8	15.9	0.22
$C_{60}Rb$	1581	8.3	12.1	1608	11.3	18.2	0.49
$C_{72}Rb$	1582	8.7	10.6	1609	8.4	18.4	0.60
$C_{1087}Rb$[b]	1582	10.8	8.0	1611	6.6	11.6	1.14
$C_{24}Cs$	—	—	—	1603	5.8	22.0	0
$C_{36}Cs$	1580	2	7.3	1605	8.3	15.2	0.12
$C_{48}Cs$	1580	4.9	8.0	1606	6.9	15.3	0.37
$C_{60}Cs$[c]	1582	4.6	9.1	1610	3.0	16.2	0.86
	1582	5.2	9.2	1607	6.6	15.8	0.47
	1582	7.1	9.9	1607	6.6	22.0	0.48
$C_{72}Cs$[c]	1581	5.7	10.5	1610	4.0	15.4	—
	1581	5.3	10.0	1610	3.1	14.1	—
	1580	5.2	10.3	1607	3.2	21.6	—
HOPG	1581	14.6	13.8	—	—	—	∞

[a] All energy values are in cm^{-1}. The amplitude, Y, is given in arbitrary units. The Raman shifts, ω, and linewidths, Γ, are accurate to $\pm 0.5\ cm^{-1}$, respectively. The linewidth Γ has been corrected for the spectral slit width. $R = I_C/I_B$ where $I\alpha$ is the integrated intensity of the Lorentzian fit to the $E_{2g}^{(2)}$ line from a type α layer, $\alpha = B, C$.
[b] The composition and stage of this sample is uncertain as indicated by the '?'.
[c] Data given for several samples which exhibited the same X-ray spectra but different Raman spectra.

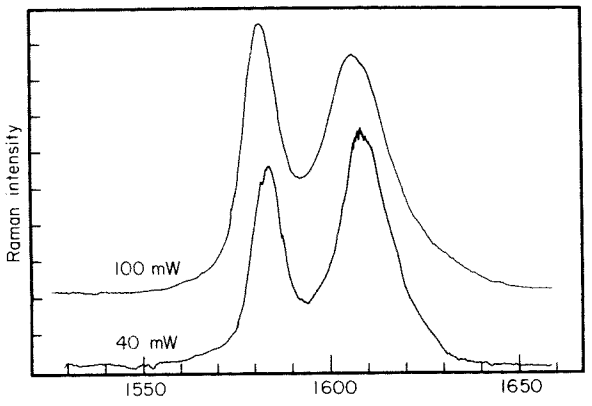

Figure 8. Two Raman spectra of a stage 5 $C_{60}Cs$ in the doublet region. With the exception of the indicated laser power, all experimental conditions for these spectra were identical.

With the exception of Cs-GIC samples, the spectrum of a particular compound shows very little variation from data set to data set, or from sample to sample. Cs-GIC samples exhibited wide variation in peak intensity and width as a function of both sample and laser power. These variations have two sources. First, the kinetics of intercalation are such that intercalation of Cs is rapid compared to K or Rb. As a result the surface of a sample may undergo intercalation or deintercalation as the sample is cooled from its preparation temperature. The (00*l*) diffraction pattern which samples the bulk (the penetration depth of MoKα radiation being $\geq$0.5 mm) indicates a pure stage, while the 1000 Å surface sampled by Raman spectroscopy is either a different stage or a mixed stage. Second the Raman spectrum appears to be very sensitive to heating by the laser beam. Figure 8 shows two Raman spectra from the same spot on a stage 5 $C_{60}Cs$ sample, with only the laser power changed. Although the relative widths of the doublet components change as a function of laser power the relative intensities remain constant. This behavior is not well understood.

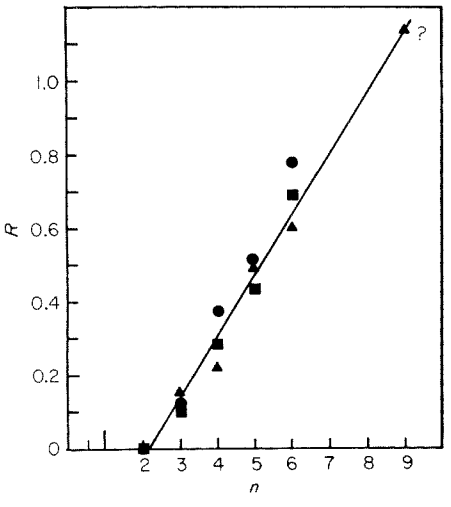

Figure 9. Plot of R v. n for $n \geq 2$ samples of K(■), Rb(▲) and Cs(●) GICs. The Cs-GIC points are an average over several (>4) samples. The line (——) is a linear least squares to the K- and Rb-GIC data points. The ratio of Raman cross sections for *B*- and *C*-type layers derived from this fit is $\sigma_C/\sigma_B = 0.25 \pm 0.05$.

The relative intensity ratio R of the NL model is plotted as a function of stage in Fig. 9 (Note that the Cs-GIC data points represent an average over several samples). To within experimental error the R values appear to be stage dependent but species independent for the heavy alkali GICs. If the total charge transferred to the carbon layers is independent of stage, the linear dependence of R with stage implies that the transferred charge remains partially localized on the *B*-type layers in agreement with the NL model. The quantity σ_C/σ_B calulated in the NL mode is constant with $\sigma_C/\sigma_B = 0.25 \pm 0.05$. This implies that the counting factor, $(n-2)/2$ accounts for all the stage dependence of R, and that therefore the NL model assumption of constant charge transfer as a function of stage is correct to within experimental error.

As expected for donor compounds $\sigma_C/\sigma_B < 1$ implying that electronic charge is transferred to *B*-type layers. In acceptor compounds $\sigma_C/\sigma_B > 1$ as has been verified for $FeCl_3$-GICs.[13] However, a detailed knowledge of the electronic band structures of the GICs formed from a given intercalant would be required to extract a fractional charge transfer per intercalate atom, f, from σ_C/σ_B. Such information is not yet available.

CONCLUSION AND SUMMARY

It is clear that Raman scattering is a useful probe for exploring vibrational excitations in GICs. Although we have concentrated here on donor compounds Raman studies of acceptor GICs have also been revealing.[16,19,39] From such studies it is known that the NL model is also applicable to acceptor GICs.[13] Moreover, some acceptor GICs—namely those formed with $FeCl_3$, and Br_2—exhibit intramolecular intercalant modes as well as the higher-frequency singlet ($n = 1, 2$) or doublet ($n \geq 3$) spectra in the 1580 cm^{-1} region.

We have shown elsewhere that significant information can be gained by studying the Raman spectrum of GICs as a function on temperature to establish what key alterations occur in the vibrational excitations as the material undergoes a structural intralayer and/or interlayer phase transition.[33] Recently Clark *et al.* have shown that when hydrostatic pressure in excess of 2 kbar is applied to stage 2 $C_{24}K$, it transforms to a stage 3 form with the same bulk stoichiometry but with a layer stoichiometry and ordered intralayer structure identical to that of C_8K.[40] Therefore it would be intriguing to study the pressure dependence of the Raman spectrum of $C_{24}K$ and to observe the evolution of the unique stage-1-like continuum spectrum.

Acknowledgements

We are grateful to A. W. Moore for providing the highly oriented pyrolytic graphite used in these studies. This research was supported by the NSF under grant No. DMR-78-11568.

REFERENCES

1. A. R. Ubbelohde and F. A. Lewis, *Graphite and Its Crystal Compounds*, Clarendon, Oxford (1960).
2. J. E. Fischer and T. E. Thompson, *Phys. Today* **31**, 36 (1978).
3. W. Rudorff and E. Schultz, *Z. Anorg. Chem.* **277**, 156 (1954).
4. *Physica* **99B** (1980) and references therein.
5. *Mater. Sci. Eng.* **31** (1977) and references therein.
6. W. Metz and D. Holwein, *Carbon* **13**, 87 (1975).
7. E. R. Falardeau, G. M. T. Foley, C. Zeller and F. L. Vogel, *J. Chem. Soc. Chem. Commun.* **11**, 389 (1977).
8. R. Clarke, N. Caswell and S. A. Solin, *Phys. Rev. Lett.* **42**, 61 (1979).
9. J. B. Hastings, W. D. Ellenson and J. E. Fischer, *Phys. Rev. Lett.* **42**, 1552 (1979).
10. H. Zabel, S. C. Moss, N. Caswell and S. A. Solin, *Phys. Rev. Lett.* **43**, 2022 (1979).
11. R. Clarke, N. Caswell, S. A. Solin and P. Horn, *Phys. Rev. Lett.* **43**, 2027 (1979).
12. W. D. Ellenson, D. Semmingsen, D. Guérard, D. G. Ohn and J. E. Fischer, *Mater. Sci. Eng.* **31**, 137 (1977).
13. S. A. Solin, *Physica* **99B**, 443 (1980).
14. *Physica* **99B** (1980) and references therein.
15. P. C. Eklund, G. Dresselhaus, M. S. Dresselhaus and J. E. Fischer, *Phys. Rev. B* **16**, 3330 (1970).
16. J. J. Song, D. D. L. Chung, P. C. Ecklund and M. S. Dresselhaus, *Solid State Commun.* **20**, 1111 (1976).
17. N. Caswell and S. A. Solin, *Solid State Commun.* **27**, 961 (1978).
18. S. A. Solin, *Mater. Sci. Eng.* **31**, 153 (1977).
19. C. Underhill, S. Y. Leung, G. Dresselhaus and M. S. Dresselhaus, *Solid State Commun.* **29**, 769 (1979).
20. N. Caswell, S. A. Solin and W. Metz, *Bull. Am. Phys. Soc.* **24**, 375 (1979) and to be published.
21. D. E. Nixon and G. S. Parry, *J. Phys. D* **1**, 291 (1968); see also, G. S. Parry, *Mater. Sci. Eng.* **31**, 99 (1977).
22. A. R. Ubbelohde and F. A. Lewis, *Graphite and Its Crystal Compounds*, Clarendon, Oxford (1960) and references therein.
23. A. Hérold, *Bull. Soc. Chim. Fr.* 999 (1955).
24. A. Hérold, *Mater. Sci. Eng.* **31**, 1 (1977).
25. R. W. G. Wycoff, *Crystal Structures*, Vol. 1, p. 26. Oxford University Press, Oxford (1962).
26. N. Caswell, S. A. Solin, T. M. Hayes and S. J. Hunter, *Physica* **99B**, 463 (1980).
27. M. S. Whittingham and L. B. Ebert, in *Physics and Chemistry of Materials with Layered Structures*, Vol. 6, *Intercalation Compounds*, ed. by F. Levy, Reidel, Dordrecht (1977) and references therein.
28. F. Tuinstra and J. L. Koenig, *J. Chem. Phys.* **53**, 1126 (1970).
29. K. K. Mani and R. Ramani, *Phys. Status Solidi B* **61**, 659 (1974).
30. R. J. Nemanich, G. Lucovsky and S. A. Solin, in *Proceedings of the International Conference on Lattice Dynamics*, ed. by M. Balkanski, p. 619. Flammarion, Paris (1978).
31. L. J. Brillson, E. Burstein, A. A. Maradudin and T. Stark, in *Physics of Semimetals and Narrow Gap Semiconductors*, ed. by D. L. Carter and R. T. Bate, p. 187. Pergamon, Oxford (1971).
32. R. J. Nemanich, G. Lucovsky and S. A. Solin, *Solid State Commun.* **23**, 117 (1977).
33. N. Caswell and S. A. Solin, *Phys. Rev. B* **20**, 2551 (1979).
34. R. J. Nemanich, S. A. Solin and D. Guérard, *Phys. Rev. B* **16** 2965 (1977).
35. M. S. Dresselhaus, G. Dresselhaus, P. C. Ecklund and D. D. L. Chung, *Mater. Sci. Eng.* **31**, 141 (1977).
36. U. Fano, *Phys. Rev.* **124**, 1866 (1961).
37. P. C. Eklund and K. R. Subbaswamy, *Phys. Rev. B* **20**, 5157 (1979).
38. C. Horie, M. Maeda and Y. Kuramoto, *Physica* **99B**, 430 (1980).
39. M. S. Dresselhaus and G. Dresselhaus, in *Physics and Chemistry of Layered Materials*, Vol. 6, ed. by F. Levy Reidel, Dordrecht (1979).
40. R. Clark, N. Wada and S. A. Solin, unpublished.

Received 15 April 1980